Solid Freeform Fabrication 2019: Proceedings of the 30th Annual International Solid Freeform Fabrication Symposium – An Additive Manufacturing Conference
Reviewed Paper

Printed Materials and Their Effects on Quasi-Optical Millimeter Wave Guide Lens Systems

Diana Foster, Chris Corey, Chris Fisher, Caitlin Smith, Dr. Arthur Paolella

All authors are affiliated with L3Harris Technologies

2400 Palm Bay Rd. NE, Palm Bay, FL 32905

Abstract

This study of 3D printed quasi-optical (Q-O) millimeter wave guide lens systems is presented in three phases: the characterization of 3D printed materials for radio frequency (RF) applications and systems; the development and demonstration of 3D printing technology for RF systems; and the design process, simulation, fabrication, and testing of RF lens systems. The first phase explores the ability to print high-quality materials with fine resolution and the determination of each material's dielectric constant and loss tangent. The second phase details the development of dual biconvex shaped lens systems and the resulting test data. The third phase combines the former stages' results to model, print, and test a set of lenses pre-aligned with an integrated support structure. These lens systems were tested up to 100 GHz with demonstrated focusing gain of 22.1 dB.

Keywords: quasi-optical, millimeter, wave guide, lens systems, radio frequency, CLIP, PolyJet, SLS, radar, space, communications

Introduction

3D printing is gaining traction for millimeter wave applications for a variety of reasons including high performance, quick design iteration time, ability to make complex geometries that are impossible for traditional manufacturing, and cost reduction. An important factor in considering the use of 3D printing is the printed material's millimeter wave performance as defined by loss tangent and dielectric constant. Loss tangent determines the dielectric loss, also referred to as dissipation factor. Dielectric constant describes the characteristic impedance of millimeter wave circuits such as quasi-optical lenses, transmission lines, and dielectric antennas [1]. Although these parameters are imperative to circuit performance, they must be assessed against the selected printing technology's ability to produce fine features of desirable accuracy and size for millimeter wave components.

Previous investigations have measured loss tangent and dielectric constant at discrete frequencies by using various techniques to 11 GHz [2] or a single method over a moderate frequency range to 10 GHz [3]. The first phase implements a two-prong approach: first, to make measurements over a broad spectrum into the millimeter wave range using a single technique from 20GHz to 57 GHz, and second, to examine various materials printed by technology most suitable for millimeter wave systems.

In the second phase, Q-O principles combined with computer-aided design (CAD) simulations are used to develop and demonstrate a functional 3D printed Q-O lens system that can efficiently couple RF energy at 39 GHz.

The third phase fabricates and tests dual biconvex lens systems for two center frequencies, 60 and 100 GHz. Biconvex lenses are selected due to the prior success of the lens system in the second phase.

I. Phase 1: Material and 3D Printing Technology Selection

a. 3D Printing Technology Descriptions and Testing Setup

Table 1 lists common materials used in the 3D printing industry and analyzed in this study. The table details the resin base type, the common commercial nomenclature, printer vendor, and printing technology. Three 3D printing technologies were used in the study: Continuous Liquid Interface Production (CLIP™), material jetting (PolyJet™) and Selective Laser Sintering (SLS). These processes were selected for the study because they can produce highly dense parts.

Table 1. 3D printed material types used in this study: ester, polyurethane, acrylate, and nylon. The materials were printed using three types of printing technology: CLIP™, PolyJet™, and SLS.

Resin Base	Resin Trade Name	Vendor	Technology
Ester	Cyanate Ester 220	Carbon	CLIP™
Polyurethane	RPU 70	Carbon	CLIP™
Polyurethane	FPU 230	Carbon	CLIP™
Acrylate	VeroWhitePlus	Stratasys	PolyJet™
Acrylate	VeroBlack	Stratasys	PolyJet™
Acrylate	VeroClear	Stratasys	PolyJet™
Acrylate	Vero Tango Blend 5	Stratasys	PolyJet™
Acrylate	Vero Tango Blend 10	Stratasys	PolyJet™
Acrylate	Vero Tango Blend 15	Stratasys	PolyJet™
Acrylate	Vero Tango Blend 20	Stratasys	PolyJet™
Acrylate	Vero Tango Blend 25	Stratasys	PolyJet™
Acrylate	Vero Tango Blend 30	Stratasys	PolyJet™
Nylon – 25% Mineral Filled	DuraForm HST	Protolab	SLS
Nylon 12 – 40% Glass Filled	PA 614-GS	Protolab	SLS
Nylon 12	PA 650	Protolab	SLS
Nylon 11	PA 850	Protolab	SLS

CLIP™ is a vat-polymerization process used by Carbon, Inc. that utilizes an oxygen-permeable window to create a "dead zone" through which ultraviolet light passes, curing the resin above the oxygen-rich layer to form a solid part. CLIP™ can produce parts with features and accuracies less than a millimeter in size over a relatively small build area (10s of centimeters). The material jetting process used in PolyJet™ printers deposits layers of liquid photopolymer onto a build tray that is simultaneously cured with an ultraviolet (UV) source. Parts produced by this method can also have features in the 100s of microns and can be up to one square meter in build

area; however, accuracy usually decreases with total part size. SLS raster scans a near-infrared laser across a powdered material bed to sinter the material into the specified geometry. While SLS printers can make parts up to a square meter build area, feature resolution is generally limited to around half a millimeter.

An open resonator technique was utilized to measure the dielectric constant and loss tangent over a wide frequency range. This technique is defined as an open configuration not completely shielded by metallic surfaces [4]. This is a well-established method and used extensively for measuring dielectric properties of materials in the millimeter wave range [5]. An additional benefit with the open resonator approach at millimeter wave frequencies allows the printed material sample size and thickness to be reasonable to fabricate. The samples need to be similar in size to the resonator reflectors yet thin enough to ensure high-frequency measurements are unaffected. The final sample geometry is 4 inches by 4 inches with a thickness of 0.020 inches (101.6mm x 101.6mm x 0.508mm).

Fig. 1 depicts how the samples were measured in the open resonator. The millimeter wave signals are incident normal to the x-y plane of the sample and the signals propagate along the z axis. The samples can also be rotated 90 degrees to determine if any results are polarization-dependent. Fig. 2 shows the major components used to tests the materials.

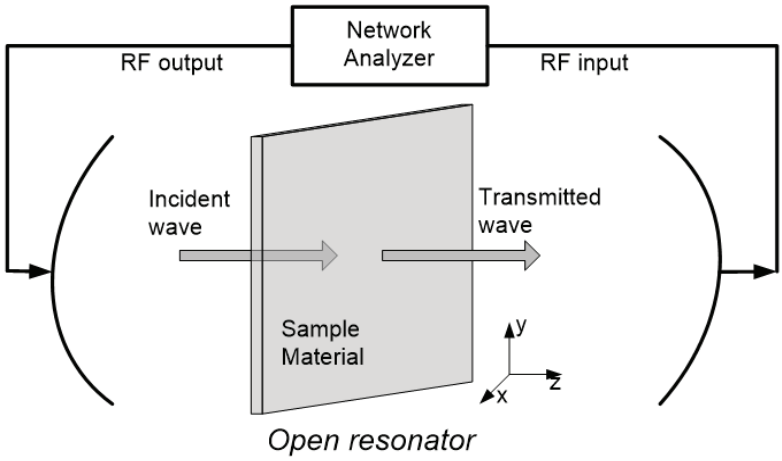

Fig. 1. Open resonator test system. The millimeter wave signal is incident to the material in the x-y plane and the signal propagates along the z axis.

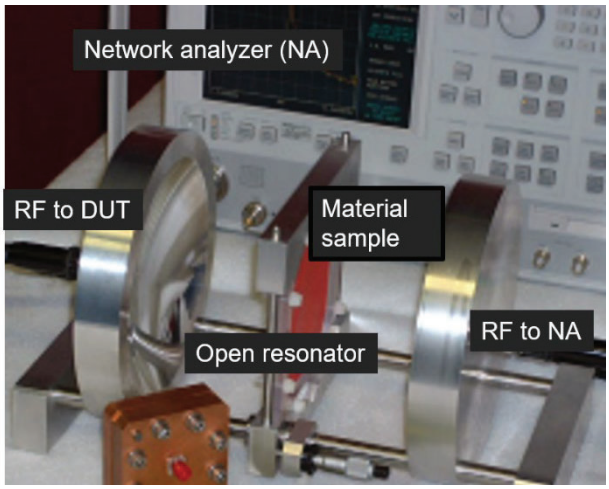

Fig. 2. Major components used in testing. Photo courtesy of Damaskos Inc.

b. 3D Printed Materials Test Results

The first set of tested materials were the acrylate-based Vero Clear blends and the Carbon Flexible Polyurethane (FPU) and Rigid Polyurethane (RPU). Fig. 3 shows the values of dielectric constant as a function of frequency. For each of these resins, the results indicate a negative slope of dielectric constant as the frequency increases. This trend is likely due to dielectric relaxation, specifically dipolar relaxation. Dipolar relaxation happens when the dielectric material is placed in an alternating electric field and the field frequency is faster than the time it takes the material's dipole moments to realign with the field. This effect results in a dielectric constant decrease as the frequency increases, as is shown in Fig. 4 [6]. The Carbon resins have much lower dielectric constants in comparison to those of the Vero resins. This gap is likely due to the chemical difference of the materials. The dielectric constant value spread for the Vero blends is most likely caused by the total doses of UV radiation. It has been shown that prolonged UV radiation exposure can alter electrical properties [7]. The loss tangent averages 0.02 over the frequency range for all these materials; this is neither remarkable nor unexpected.

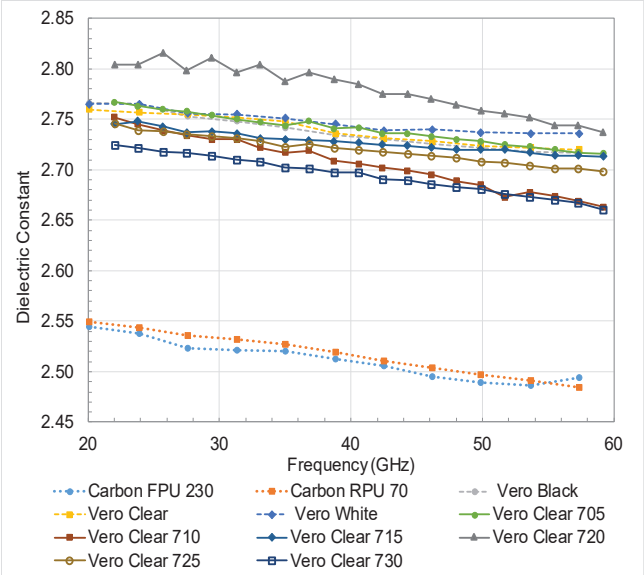

Fig. 3. Acrylate and polyurethane grouping. These materials display a negative slope as a function of frequency due to dielectric relaxation.

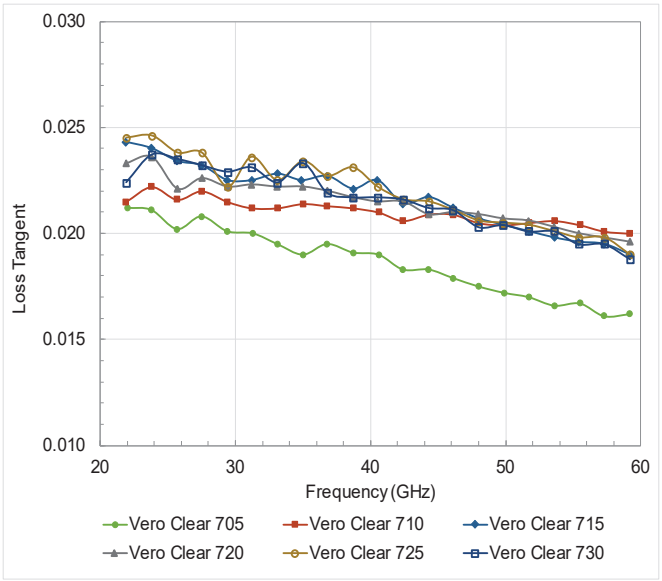

Fig. 4. Acrylate grouping. The loss tangent of the materials displays a negative slope with frequencies.

The same negative slope exists in loss as it does in the dielectric constant. The acrylate-based resins are highly polarizable at the applied field frequencies [6]. Thus, the material has many resonance peaks. The chance of interacting with a resonance peak is higher within the frequency range studied. There tends to be greater absorption in the material if the applied field frequency is near a resonance peak, resulting in higher losses. The main difference among all the Vero Clear material blends is the amount of flexible polymer added during the printing process. Vero Clear 705 has the lowest amount of flexible polymer and Vero Clear 730 has the highest. If the flexible polymer is more strongly polarizable than the clear rigid polymer, this explains why the blends

with more flexible material show more loss at a given frequency. This effect is more pronounced at lower frequencies due to the quantity of resonance peaks or the peak strength.

The second set of tested materials was polyamide-based powders. PA 614-GS and PA 650 are nylon 12 powders with PA 614-GS being 40% glass filled. PA 850 is an unfilled nylon 11 material. DuraForm HST is a nylon-based material filled with fine mineral powder. The values of dielectric constant as a function of frequency for these materials are shown in Fig 5. PA 614-GS has a higher dielectric constant in comparison to PA 650 and PA 850 as the volume fraction of glass filler in PA 614-GS has a higher dielectric constant (generally 5-10) than the bulk nylon material. The variance in dielectric constant between PA 650 and PA 850 is a result of polymer structure, specifically the difference in carbons present in the repeat unit of the polymer. Nylon polymers with an even number of carbons (e.g., nylon 12) have alternating linkages (-CONH-) which cause the dipole moments to cancel when an electric field is applied, thereby decreasing the dielectric constant [8]. Nylon polymers with an odd number of carbons (e.g., nylon 11) do not have this molecular symmetry. Therefore, the dipole moments do not cancel, resulting in a higher dielectric constant [9]. Nylon 11 is expected to have a higher dielectric constant than nylon 12, and this is supported by the presented data for PA 850 and PA 650. DuraForm HST exhibits the highest dielectric constant out of the second set. This is most likely due to the mineral filling being inorganic. A few examples of minerals used to fill nylon are mica, silica, and calcium carbonate. The specific mineral used to fill the nylon can greatly affect the dielectric constant; however, the filler used in DuraForm HST is unknown at the time of this experiment. These materials show low loss tangent compared to the acrylate- and polyurethane-based resins as depicted in Fig. 6.

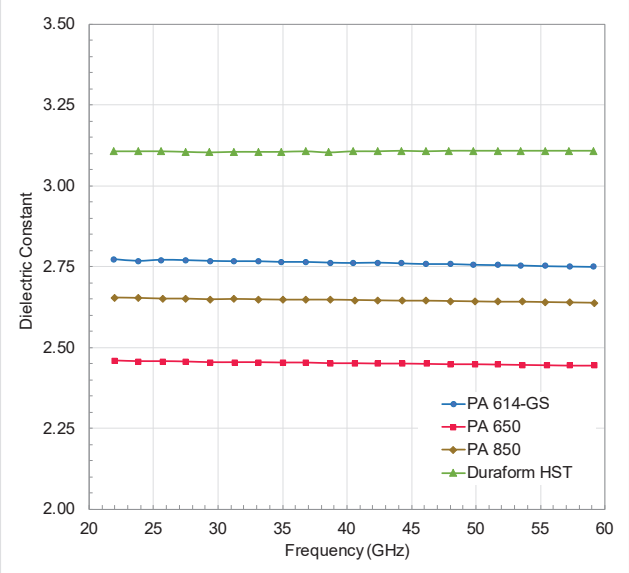

Fig. 5. Polyamide grouping. Polyamide-based material dielectric constants as a function of frequency.

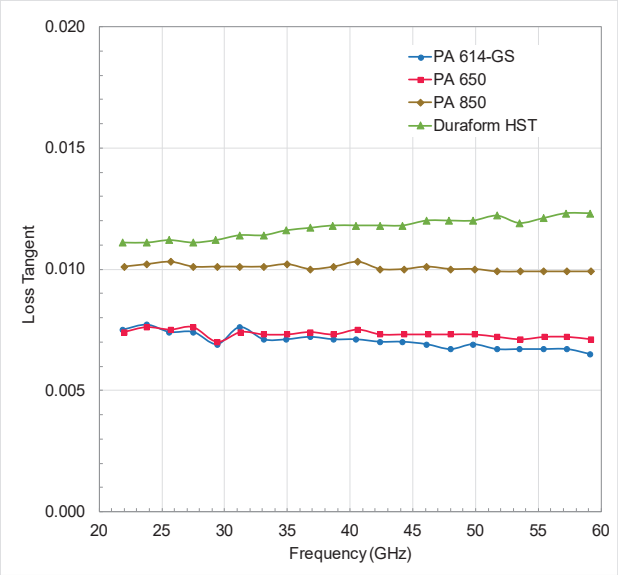

Fig. 6. Polyamide grouping. Polyamide-based material loss tangent as a function of frequency.

The last material tested was Carbon's CE220. This was selected because passive millimeter wave components, such as lenses and antennas, can be made with high resolution and low surface roughness using the CLIP process. The results in Fig. 7 exhibit a flat dielectric response with frequency and moderate loss.

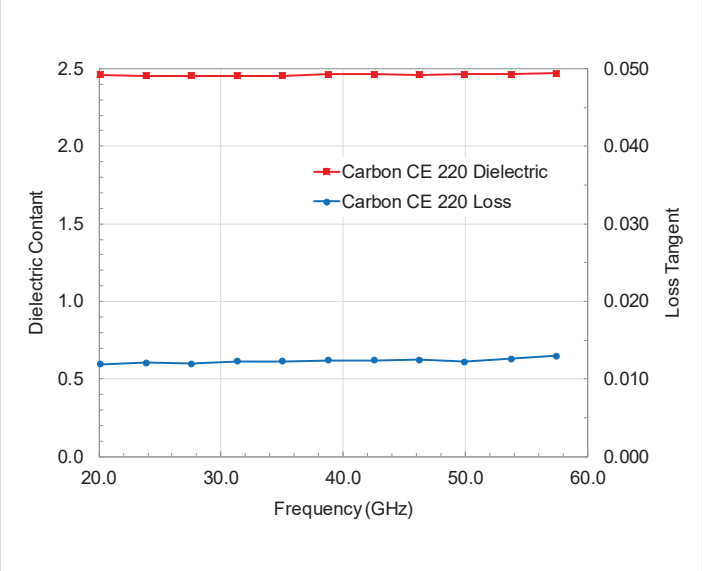

Fig. 7. CE 220 material dielectric constant and loss tangent as a function of frequency. The data shows flat response of the dielectric constant as well as moderate loss tangent.

II. Phase 2: 3D Printed Q-O Lens Systems for 39 GHz Application

a. Q-O Lens Design and Simulation

Following the first phase's characterization of 3D printable materials, cyanate ester 220 (CE 220) was chosen to print using the Carbon M1 CLIP technology as it provides the best dielectric constant and loss tangent and minimum producible feature size that can be printed in-house. By the time printing commenced, Carbon had updated the CE 220 material to CE 221, which maintains the material properties with the benefit of easier printability and post-processing. For the lens design, Q-O principles in combination with computer-aided design (CAD) were used to create and demonstrate a functional single-print lens system with integrated support structure as shown in Fig. 8.

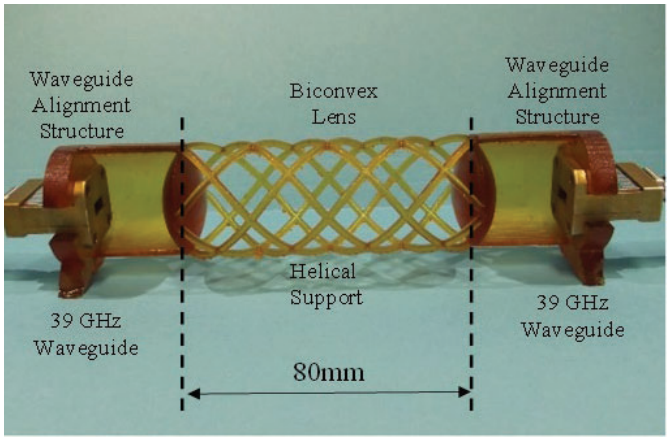

Fig. 8. Single-print biconvex lens system with integrated support structure. The two lenses are separated by 80 mm with 120 mm space between the waveguides.

The first step in designing Q-O lens systems was to specify system parameters and desired values to reduce the problem complexity. The design is constrained by the build volume of the Carbon M1 printer; thus, the experiment was performed across 15 wavelengths of separation between the waveguides which is the maximum amount contained in the build volume. The lens designs began with diameters on the order of three wavelengths as seen in the lens designs [2]. Zeroth order designs were made by combining the lens maker's equation, geometrical optics, and physical optics principles as reported in [10]. The lenses have identical design. The subsequent step is to model the lens systems in an electromagnetic propagation simulation software once these principles establish the systems' zeroth order approximation. The body (cavity) boundaries were treated as radiation boundaries and the input and output waveguides were modelled as perfect electrical conductors. The results of one simulation are shown in Fig. 9.

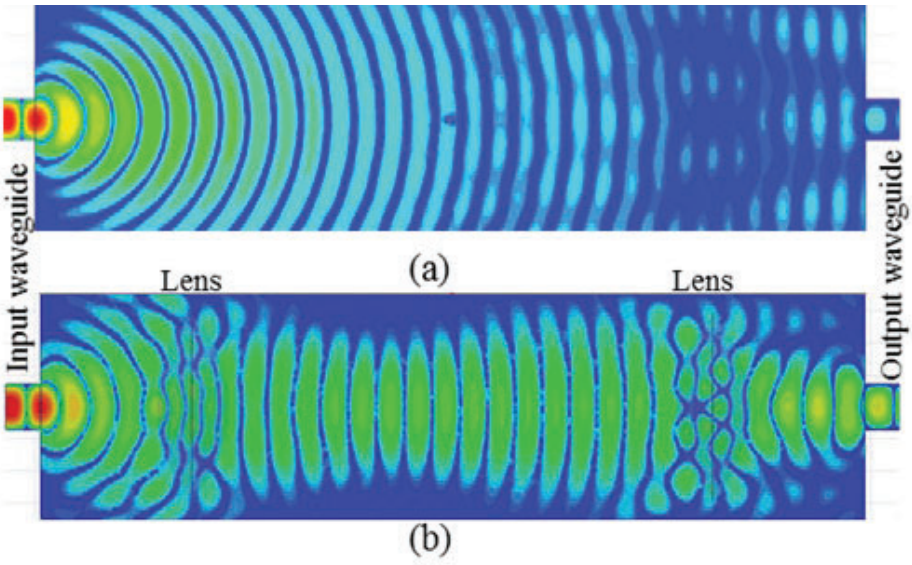

Fig. 9. Electromagnetic propagation simulation. (a) Free space cavity with 120 mm separation between waveguides, and (b) the biconvex lens system with 80 mm separation between lenses and 120 mm separation between the waveguides.

Initial tests were performed on the single-print lens system with integrated support structure. Afterwards, a new design was developed to allow for control of lens spacing during testing, improved resolution of the printed lenses, and to reduce support structure interference with the propagating RF wave. The new design used the same lens specifications but was printed with a higher resolution, resulting in a smoother lens surface. The cavity body was also designed to maintain rigid alignment of the attached waveguides and allow easy placement of the lens while reducing the amount of cross section near the lenses. New simulations were completed for this system at 39 GHz. The two lenses and cavity body were printed and assembled for testing as shown in Fig. 10.

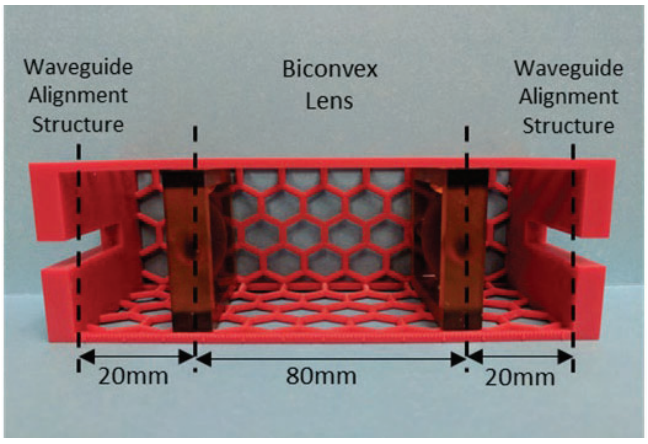

Fig. 10. Separated body and lens design. The two lenses were printed at a higher resolution than the single-print system and the body maintains rigid alignment of the input and output waveguides.

b. Q-O Lens System Test Results at 39 GHz

The lens system was tested using a broadband vector network analyzer (VNA) to couple signals from 35 to 43.5 GHz across the 120 mm gap. The results are shown in Fig. 11 for both the single-print biconvex lens system and an empty free-space cavity of equal length for comparison. The observed ripple can be attributed to the open waveguides as no attempt was made to optimize or match the outputs. The single-print lens system shows a measured gain of 12.9 dB over the free-space equivalent system. This aligns well with the simulation results to within 2 dB. This mismatch is likely to be attributed to slight printing errors on the surface of the lenses and small misalignments which occurred during the curing process for the CE 221 material.

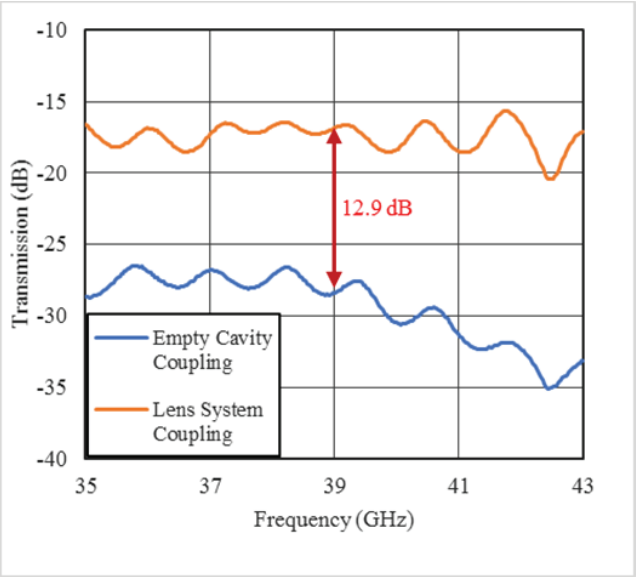

Fig. 11. Measured results of the single-print biconvex lens system, demonstrating a 12.9 dB gain.

This stage of design development provides knowledge of improvements to the printing process and design methodology which is applied to the second iteration of the lens system. The separate lens and body cavity design exhibits better gain than the integrated support design, achieving a gain of 18.6 dB over the empty free-space equivalent system as seen in Fig. 12. The increased gain over the fixed alignment structure could be due to improvements in lens alignment, elimination of alignment and support structure, and increased printer resolution. Lenses from both systems have the same design.

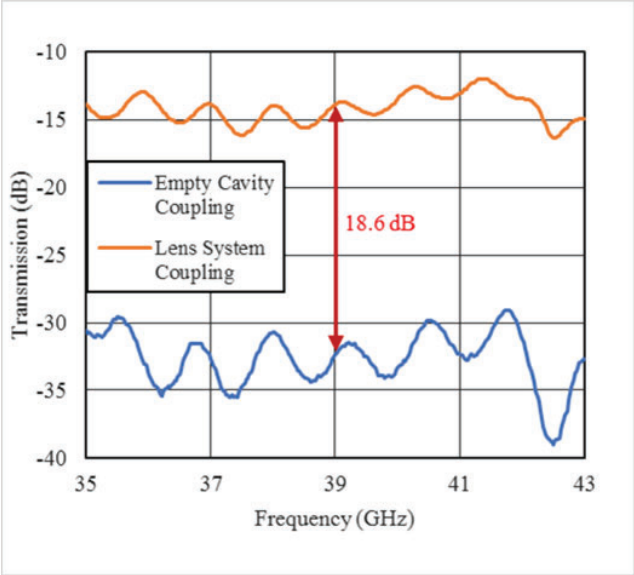

Fig. 12. Measured results of separate print lens and cavity body system, demonstrating an 18.6 dB gain.

III. Phase 3: 3D Printed Q-O Lens Systems for 60 and 100 GHz Applications

a. Q-O Lens Design and Simulation

As in Phase 2, the first step taken in the Q-O lens systems design was to determine the desired system parameters. The center frequencies of 60 and 100 GHz were chosen, and it was decided to perform the experiment with a separation of 15 wavelengths between lenses. The initial lens designs had diameters on the order of three wave lengths [3,11] and thicknesses between 5 and 10 millimeters. These thicknesses were used to figure out the interplay between the coupling surface size and the energy coupled to derive the minimum size the lens can be while remaining effective. Zeroth order designs created using design principles from [12]-[16] take into consideration the same candidate material and 3D printing methodology used in Phase 2.

After the first design iteration, a geometrical optics approach was applied to confirm the designs and improve their accuracy. Ray tracing was completed using Snell's law to find the approximate image locations and system magnifications. Next, the total systems magnifications were calculated to ensure the RF energy collimated at the output falls within the system output coupling waveguide aperture. The systems were then modelled in an electromagnetic propagation simulation software. Again, an empty cavity was also simulated for comparison of the effectiveness of the lens systems over free-space coupling. The lens systems were simulated with parametric sweeps near the initial values to find the optimal lens size, radii, thickness, and spacing needed to achieve optimal coupling. The electric field profiles of the optimized lens systems in addition to the free-space cavity propagation can be seen in Fig. 13.

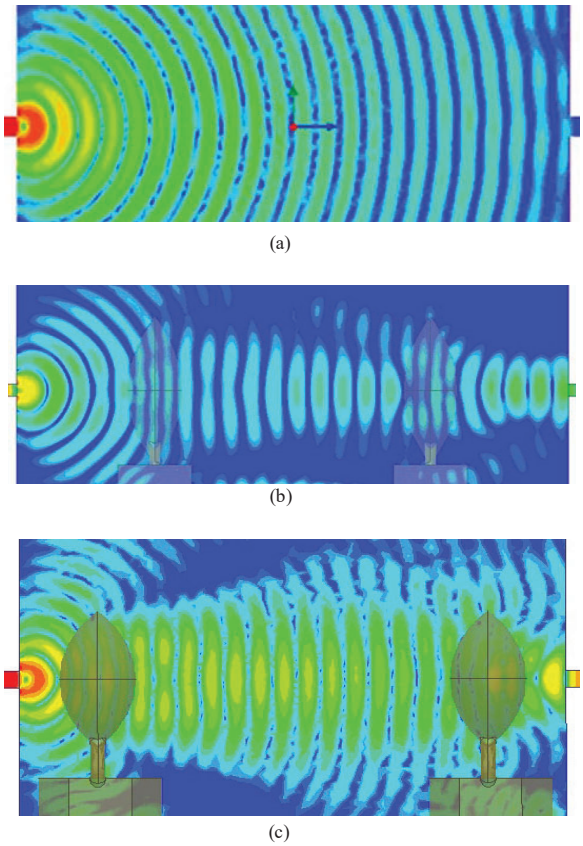

Fig. 13. Electromagnetic simulations of (a) empty cavity, (b) 60 GHz lens systems, and (c) 100 GHz lens system.

The final design parameters were exported to modelling software once the simulations converge. Rigid plastic components were created to provide alignment and ease of spacing manipulation for the lenses along multiple interlock points. Support and alignment structures were also designed for both frequencies. The 60 GHz lens was large enough to print with a simple integrated rectangular support structure, as shown in Fig. 14(a). The 100 GHz lens needed an elongated pedestal support structure to ensure the lens rested within the center of the cavity, shown in Fig. 14(b). Simulations including the support and alignment features were completed and the system response was characterized at multiple frequencies to provide a broad picture of the performance measured from the actual device.

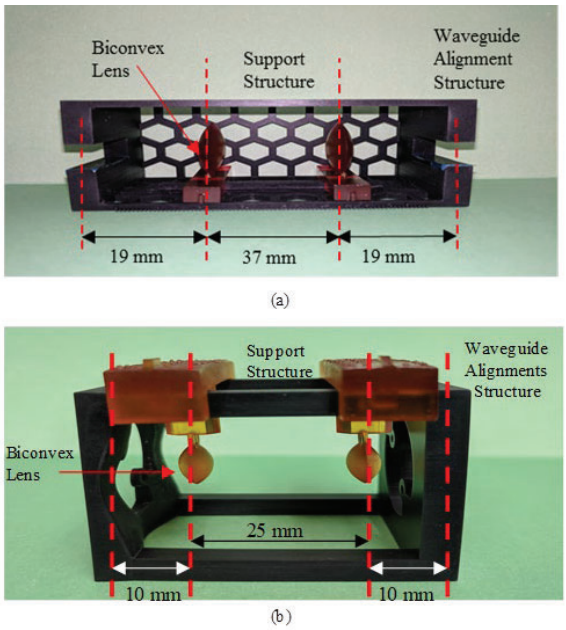

Fig. 14. 3D printed lens systems for (a) 60 GHz design and (b) 100 GHz design.

The rigid body cavities were printed first and used to measure transmission performance when the space between the output waveguides is an open-space air cavity. After the reference value was confirmed to be a match for the simulation results, the lenses were printed and the alignment tested to ensure the lenses' placement was accurate and consistent with the intended design parameters. The 60 GHz lens was tested using a VNA transmitting from 50 to 67 GHz through an output and subsequent input of V-band waveguide to coaxial connectors. The resulting S_{21} transmission measurement was collected across the entire frequency span. The data was collated and compared to the free-space cavity result to find the gain from the addition of the lenses. The 100 GHz lens necessitates the use of RF mixers to create the 100 GHz tone and then re-measure it after the system output. The mixer intermediate frequency signal was changed at regular intervals to provide transmission values across frequencies from 90 to 110 GHz. This was used for comparison against the simulation broad spectrum results.

b. Q-O Lens System Test Results at 60 and 100 GHz

In simulation, the 60 GHz lens system was predicted to have a gain of 19.5 dB over the free-space cavity system. The printed lens system was tested to have a gain of 18.3 dB over the free-space cavity. The difference of 1.2 dB could be attributed to slight printing errors on the surface finish of the lenses as well as lens misalignment. The 100 GHz lens system simulation predicted a gain of 22.3 dB over the free-space cavity. The printed lens system resulted in a gain of 22.1 dB. The 0.2 dB difference could be attributed to slight printing errors on the surface finish of the lenses. The accuracy improvement of the 100 GHz system over the 60 GHz system is due to the superior mechanical structure of the 100 GHz cavity body allowing more exact placement of the lenses. The 100 GHz cavity body features built-in alignment structures, locking the lenses into position and, thus, reducing variability. Experimental results are shown in Table 2.

Table 2. Comparing simulation gain results and measured gain results.

Frequency (GHz)	Simulated Gain (dB)	Measured Gain (dB)
60	19.5	18.3
100	22.3	22.1

Discussion

The three phases presented in this study cover the determination of material millimeter wave properties, the initial design and testing of a biconvex Q-O lens system at 39 GHz, and the refined design and testing of biconvex Q-O lens systems at 60 and 100 GHz.

In Phase 1, four groups of materials were analyzed: ester, polyurethane, acrylate, and nylon. The dielectric constant of these materials varied between 2 and 3. Both the polyurethane and acrylate groups show a negative slope of the dielectric constant with frequency that can be attributed to polymer chain structure. The ester and nylon groups show generally flat responses across the tested frequencies. The loss tangent of all material groups was in the range of 0.02; however, the nylon-based materials have much lower loss, down to 0.007. Although millimeter wave parameters are pertinent to circuit performance, they must be weighed against current 3D printing technology's ability to render fine features of suitable size and accuracy for millimeter wave components.

Phase 2 of the study used the results from Phase 1 and applied them to the design, simulation, and testing of Q-O lens systems. At 39 GHz, a noticeable gain of 18.6 dB over the free-space equivalent system was observed.

Finally, Phase 3 looked to build upon the findings of Phase 2. New design considerations were implemented, resulting in a measured gain of 18.3 dB and 22.1 dB over the free-space equivalent system for 60 and 100 GHz, respectively.

Conclusion

The data collected from each phase prove promising in the viability of this technology to produce a functional biconvex Q-O lens system capable of shaping the wave front. Applications for this technology include combining spatial power for systems operating at millimeter wave through terahertz frequencies. Further enhancements to these systems can be completed with improvements in material properties and characteristics, specifically loss tangent, and in printing method to reduce surface roughness. Conceptual designs not producible through traditional manufacturing techniques are now available to engineers. The ability to make millimeter wave components in-house, both quickly and at low cost, provides interesting new means for affordable and rapid commercialization. 3D printing lends substantial weight behind the initiative to further develop this technology.

References

[1] J. Harvey, A. Paolella, M. B. Steer, and J. W. Mink, "A quasi-optical dielectric slab power combiner," *IEEE Microwave and Guided Wave Letters*, vol. 6, no. 2, Feb. 1996.

[2] P. I. Deffenbaugh, R. C. Rumpf, and K. H. Church, "Broadband microwave frequency characterization of 3-D printed materials," *IEEE Transactions on Components, Packaging, and Manufacturing Technology*, vol.3, no. 12, pp. 2147-2155, Dec. 2013.

[3] P. I. Deffenbaugh, T. M. Weller, and K. H. Church, "Fabrication and microwave characterization of 3-D printed transmission lines," *IEEE Microwave and Wireless Components Letters*, vol. 25, no. 12, Dec. 2015.

[4] G. Annino, T. Kolodiazhnyi, and M. Martinelli, "Open resonators for millimeter wave spectroscopy," *2007 International Kharkov Symposium Physics and Engrg. of Millimeter and Sub-Millimeter Waves (MSMW).* vol. 1, pp. 109 – 114, 2007.

[5] Suzuki, H., Kamijo,T, "Millimeter-Wave Measurement of Complex Permittivity by Perturbation Method Using Open Resonator," *IEEE Transactions on Instrumentation and Measurement*, Volume: 57, Issue: 12, Dec. 2008.

[6] Z. Ahmad (2012). Polymer dielectric materials, dielectric material, Dr. Marius Alexandru Silaghi (Ed.), InTech. [Online] Available: https://www.intechopen.com/books/dielectric-material/polymer-dielectric-materials

[7] Y. Wang and T. Hsieh, "Effect of UV curing on electrical proper-ties of a UV-curable co-polyacrylate/silica nanocomposite as a transparent encapsulation resin for device packaging," *Macromol. Chem. Phys*., 2007.

[8] J. S. Harrison and Z. Ounaies, "Piezoelectric Polymers," in *Encyclopedia of Polymer Science and Technology*. New York: John Wiley and Sons, 2002.

[9] G. Wu, O. Yano, and T. Soen, "Dielectric and piezoelectric proper-ties of nylon 9 and nylon 11," *Polymer Journal*, vol. 18, no. 1, 1986.

[10] P.F. Goldsmith, "Quasi-optical techniques at millimeter and submillimeter wavelengths", *Infrared and Millimeter Waves*, K. J. Button, Ed. New York: Academic, 1982, vol. 6, Ch. 5.

[11] R. Ernst, et al, "60 GHz vital sign radar using 3D-printed lens", *Sensors*, 2016, ISBN 978-1-4799-8287-5/16.

[12] C. W. Hicks, H-S Hwang, M. B. Steer, J. W. Mink, J. F. Harvey, Member, "Spatial Power Combining for Two-Dimensional Structures," *IEEE Transactions on Microwave Theory and Techniques*, vol. 46, no. 6, pp. 784-791, Jun. 1998.

[13] N. Dolatsha, et al, "17.8 A compact 130GHz fully packaged point-to-point wireless system with 3D-printed 26dBi lens antenna achieving 12.5Gb/s at 1.55pJ/b/m", Solid-State Circuits Conference 2017.

[14] D. Guo, et al, "A terahertz quasi-optical detector based on a 3D printing lens," 2015 IEEE MTT-S International Microwave Workshop Series on Advanced Materials and Processes for RF and THz Applications (IMWS-AMP).

[15] Ran Yang, et al, “Study on Integrated Lens for 220 GHz Quasi-Optical Mixers” 2014 3rd Asia-Pacific Conference on Antennas and Propagation, Harbin, China, 26 Jul - 29 Jul 2014.

[16] Electronic System Including Waveguide with Passive Optical Elements and Related Methods, U.S. Patent Application No. 15/492,317, April 20, 2017.